Supporting Information

Rational construction of covalent organic frameworks with multiple-site functional groups for highly efficient removal of low-concentration U(VI) from water

Tingting Yang [a], Chen Tian[*b, c], Xu Yan [b, c], Ruiyang Xiao [b, c] and Zhang Lin [a, b, c]

a. School of Environment and Energy, Guangdong Provincial Key Laboratory of Solid Wastes Pollution Control and Recycling, South China University of Technology, Guangzhou, Guangdong 510006, China.
b. School of Metallurgy and Environment, Central South University, Changsha, Hunan 410083, PR China.
c. Chinese National Engineering Research Centre for Control and Treatment of Heavy Metal Pollution, Changsha, Hunan 410083, PR China.

***Corresponding author:** Chen Tian

E-mail: birdytc@hotmail.com (Dr. Chen Tian)

Content

S1. Materials and Reagents

2,4,6-Trihydroxy benzene-1,3,5-Tricarbaldehyde (doted as Tp) (> 98%) and 2,5-diaminobenzene-1,4-dicarbonitrile (doted as Dd) (> 98%) were purchased from Tengqian Biotechnology Co. Ltd, Shanghai, China. Anhydrous mesitylene (98%), hydroxylamine hydrochloride (98.5%), anhydrous dioxane (≥ 98.5%), sodium hydroxide, nitric acid, and acetic acid (≥ 99.7%) were purchased from Aladdin Industry Co. Ltd., Shanghai, China. Trimethylamine (about 25% in methanol, about 3.2 mol L^{-1}) was purchased from TCL. Anhydrous methanol was purchased from Sinopharm group. And all reagents were used without further purification. The uranium stock solution was prepared by dissolving the appropriate amount of $UO_2(NO_3)_2 \cdot 6H_2O$ in deionized water. Deionized water used in all the experiments was obtained from a Milli-Q water purification system.

S2. Characterization

X-ray diffraction (XRD) data were collected by a D8-Advance X-ray diffractometer (Bruker, German) with a high-intensity monochromatic nickel filtered Cu Kα (λ = 1.5406 Å) radiation. The Fourier-transform infrared (FT-IR) spectra of the samples were recorded on an RX1 PerkinElmer FT-IR spectrometer using KBr as a diluent. The solid-state ^{13}C NMR spectra were recorded on an Agilent 600 (600 MHz) spectrometer at ambient temperature, the chemical shifts were referenced to TMS. Brunauer-Emmett-Teller (BET) specific surface area (SSA) of the samples was determined by collecting N_2 gas adsorption/desorption isotherms on a Micromeritics ASAP 2020 Instrument. Before the SSA determination, all samples of COFs were degassed at 120 °C for 10 h. The specific surface areas for N_2 were calculated under the N_2 pressure ($0.005 < P/P_0 < 0.1$). The pore size distributions were calculated from the adsorption-desorption isotherms via density functional theory (DFT) and Barrett-Joyner-Halenda (BJH) model. Thermogravimetric analysis (TGA) experiments data were collected using STA 449C simultaneous thermal analyzer (NETZSCH, Germany). 10 mg samples were heated from 30 to 800 °C with a heating rate of 10 °C min^{-1} under the nitrogen atmosphere. Scanning electron microscopy (SEM) images were collected using a Hitachi SU 1510 and SU 4800. The XPS spectra were recorded by an Axis Ultra DLD instrument (Kratos Analytical, U.K.) using an A1 Kα X-ray source, at pass energy of 160 eV for survey scans and 40 eV for higher solution scans. The residual concentration of uranium was measured by inductively coupled plasma mass spectrometry (ICP-MS, PerkinElmer, USA) and inductively coupled plasma optical emission spectrometry (ICP-OES, PerkinElmer, USA).

S3. Adsorption models

To further understand the adsorption equilibrium of the absorbents, Langmuir (eq 1) and Freundlich models (eq 2) were employed to fit the isotherms on uranium adsorption by COFs after adsorption for 12 h. The adsorption isotherms fitted with the following equations:

$$\frac{C_e}{q_e} = \frac{C_e}{Q_{max}} + \frac{1}{Q_{max}K_L} \quad (1)$$

where Q_{max} and K_L are Langmuir constants, corresponding to the maximum adsorption capacity at complete monolayer coverage (mg g^{-1}) and the Langmuir affinity coefficient (L mg^{-1}); C_e and q_e are the equilibrium concentration of adsorbate (mg g^{-1}) and amount adsorbed at equilibrium (mg g^{-1}), respectively.

$$q_e = K_F \times C_e^n \quad (2)$$

where q_e is the adsorption capacity of the adsorbent (mg g^{-1}), C_e is the equilibrium concentration (mg L^{-1}), and K_F and n are the Freundlich constants characteristic of an adsorption isotherm.

To evaluate the adsorption kinetics and mechanism of the adsorbents, pseudo-first-order, pseudo-second-order were used to fit the kinetics on uranium adsorption by COFs after adsorption for 12 h. The adsorption kinetics fitted with the following equations:

$$\ln\left(q_e - q_t\right) = lnq_e - k_1 \times t \quad (3)$$

where q_t (mg g^{-1}) and q_e (mg g^{-1}) are the amounts of adsorbed uranium at the contact and equilibrium times, respectively, t is the contact time (min), and k_1 is the rate constant (min^{-1}).

$$\frac{t}{q_t} = \frac{1}{k_2 q_e^2} + \frac{t}{q_e} \quad (4)$$

where q_t (mg g^{-1}) and q_e (mg g^{-1}) are the amounts of adsorbed uranium at the contact and equilibrium times, respectively, t is the contact time (min), and k_2 is pseudo-second-order adsorption rate constant (g mg^{-1} min^{-1}).

The selectivity coefficient ($\beta_{UO_2^{2+}/M^{n+}}$) for uranium, as a specific term to describe the potency and degree of selectivity of the adsorbent,[1] was calculated by the following equation:

$$\beta_{UO_2^{2+}/M^{n+}} = K_{d(UO_2^{2+})}/K_{d(M^{n+})} \quad (5)$$

$$K_d = Q_e/C_e \quad (6)$$

where C_e is the equilibrium concentration (mg L^{-1}), Q_e is the adsorption capacity of the adsorbent (mg g^{-1}).

S4. Supplemental Results

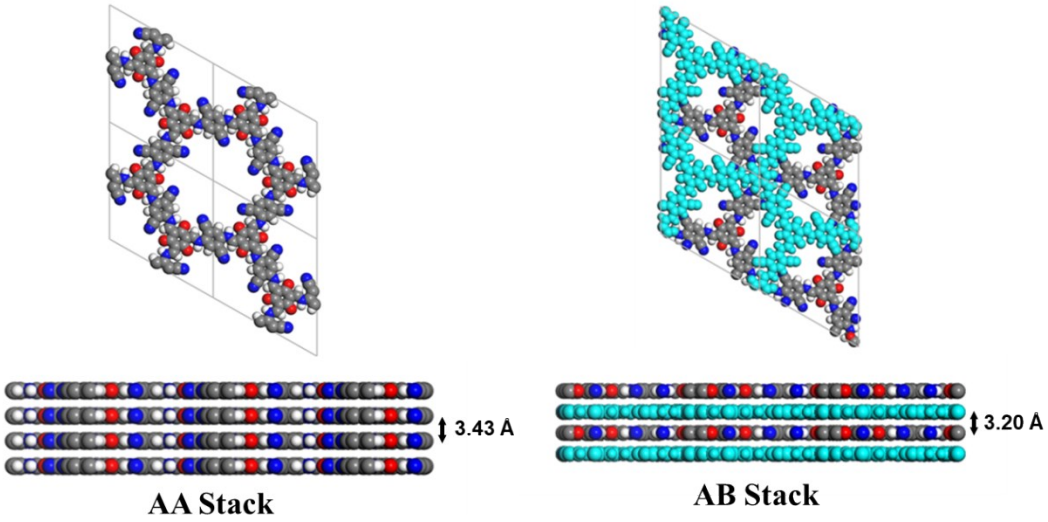

Fig. S1. The AA Stack and AB Stack Model of COF-TpDd from the top and side view and their corresponding layer spacing.

Table. S1. Atomistic coordinates for the unit cell for the AA-stacking mode of COF-TpDd optimized using the Forcite method (space group P-6, a = b = 21.4535 Å; c = 3.4302 Å, α = β = 90° and γ = 120°).

Atom	X	Y	Z
C1	0.38324	-0.19226	0
C2	0.36215	-0.25869	0
C3	0.28757	-0.30402	0
O4	0.27716	-0.47189	0
N5	0.40706	-0.45271	0
C6	0.45713	-0.47253	0
C7	0.42752	-0.54431	0
C8	0.46767	-0.57503	0
C9	0.42383	-0.65232	0
N10	0.61135	-0.28727	0
H11	0.3447	-0.17821	0
H12	0.35633	-0.49368	0
H13	0.37079	-0.5785	0

Table. S2. The comparison of the stability test conditions of COF-TpDd-AO_2 with other COFs reported in the literature.

Materials	Chemical Stability	References
COF-TpDb-AO	Saturated NaCl、HCl (3 M)、NaOH (3 M); T = 24 h	2
COF-JLU2	HNO_3 (5 M)、NaOH (5 M); T = 24 h	3
COF-PDAN-AO	HCl (5 M)、NaOH (5 M); T = 6 h	4
TFPT-BTAN-AO	HCl (1 M)、NaOH (1 M)、HNO_3 (0.1、0.5、1、3、5 M); T = 12 h	5
TP-COF-AO	HNO_3 (3 M)、NaOH (3 M); T = 24 h	6
SCU-COF-1	HCl (1 M)、HNO_3 (1 M、3 M)、NaOH (1 M); T = 24 h	7
TAPB-BMTTPA-COF	HCl (6 M)、NaOH (6 M); T = 72 h	8
COF-V	HCl (1 M)、NaOH (2 M); T = 24 h	9
Redox-COF1	HNO_3 (pH = 1.0-7.0); T = 72 h	10
TpODH	HCl (9 M)、NaOH (9 M); T = 24 h	11
This Work	**HNO_3 (1、3、5 M)、NaOH (1、3、5 M); T = 24 h**	/

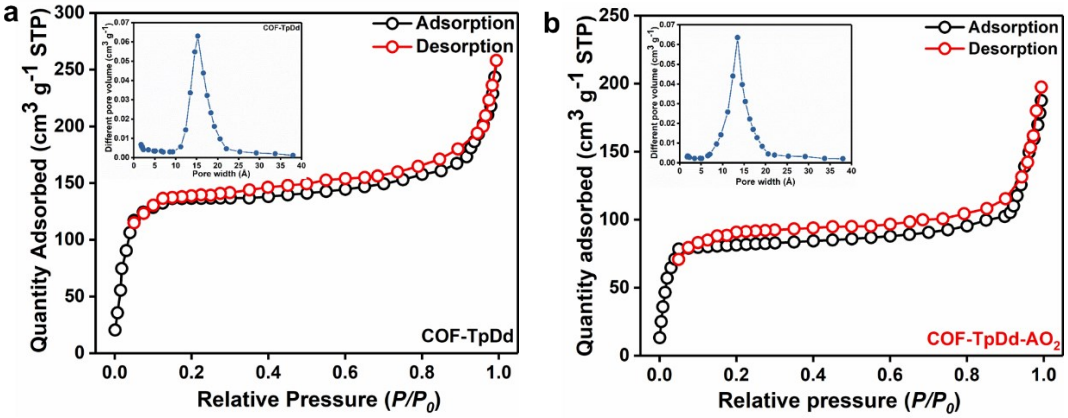

Fig. S2. The nitrogen adsorption isotherm and pore size distribution of COF-TpDd (a) and COF-TpDd-AO_2 (b).

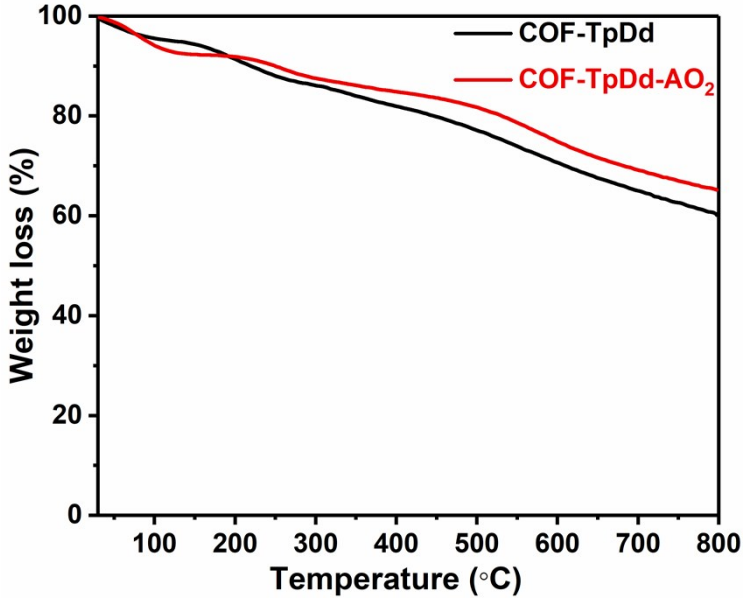

Fig. S3. Thermogravimetric analysis of COF-TpDd and COF-TpDd-AO_2 under the nitrogen atmosphere with the heating rate of 10 °C min^{-1} at 30-800 °C.

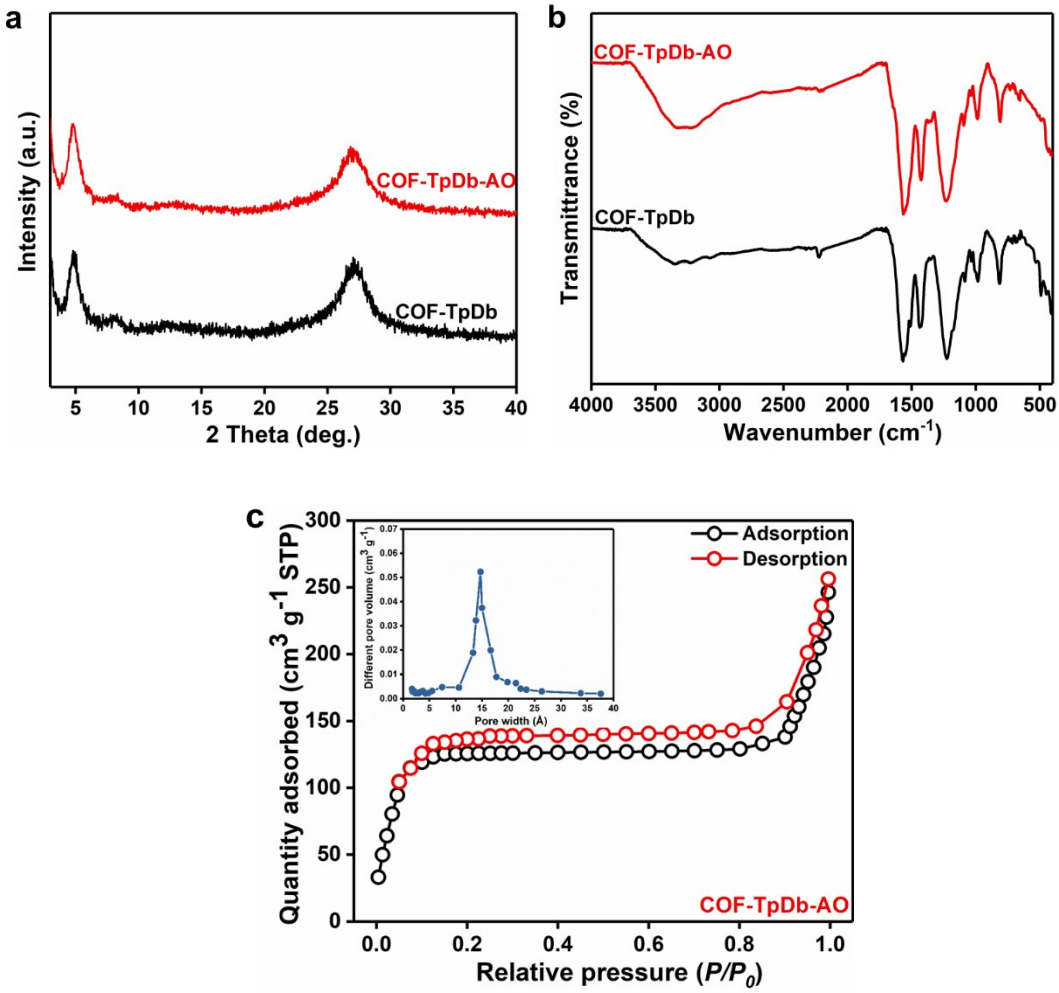

Fig. S4. The XRD (a), FT-IR (b) and N_2 adsorption/desorption curves (c) of COF-TpDb-AO.

Table. S3. The Langmuir model and Freundlich model for uranium absorbed onto COFs, C_0 = 0.2-10 mg L^{-1}; COFs included COF-TpDd, COF-TpDb-AO and COF-TpDd-AO_2.

Uranium	Absorbents	Langmuir model			Freundlich model		
		Q_{max} (mg g^{-1})	K_L (L mg^{-1})	R^2	K_f ($mg^{1-n}\cdot L^n\cdot g^{-1}$)	n	R^2
Part A	COF-TpDd	0.83	33.82	0.7398	2894.42	1.90	0.9929
	COF-TpDb-AO	0.99	42.68	0.9826	3736.37	1.75	0.9972
	COF-TpDd-AO_2	1.70	229.15	0.9632	14228.61	1.47	0.9993
Part B	COF-TpDd	19.14	4.25	0.9935	20.01	0.61	0.9811
	COF-TpDb-AO	18.38	6.39	0.9907	22.02	0.57	0.9811
	COF-TpDd-AO_2	16.62	26.04	0.9902	24.97	0.43	0.9864
Part C	COF-TpDd	40.21	0.39	0.7439	26.19	1.48	0.9957
	COF-TpDb-AO	40.29	0.48	0.9008	35.26	1.48	0.9954
	COF-TpDd-AO_2	27.50	0.96	0.9888	82.91	1.71	0.9926
Part D	COF-TpDd	41.79	1.39	0.9988	24.45	0.27	0.9969
	COF-TpDb-AO	48.88	1.60	0.9975	27.19	0.31	0.9970
	COF-TpDd-AO_2	49.02	2.16	0.9984	31.61	0.27	0.9893

Table. S4. Kinetic parameters for pseudo-first-order model, pseudo-second-order model for uranium with the concentrations of 0.5 and 5 mg L^{-1} adsorbed onto COFs; COFs included COF-TpDd, COF-TpDb-AO, and COF-TpDd-AO_2.

Initial Concentration	Absorbents	Pseudo-first-order model			Pseudo-second-order model		
		Q_e (mg g^{-1})	k_1 (min^{-1})	R^2	Q_e (mg g^{-1})	k_2 (g $mg^{-1}min^{-1}$)	R^2
0.5 mg L^{-1}	COF-TpDd	1.40	0.0504	0.9387	2.36	0.1233	0.9999
	COF-TpDb-AO	1.15	0.0578	0.9362	2.44	0.1462	0.9999
	COF-TpDd-AO_2	1.19	0.0832	0.9596	2.79	0.1473	0.9998
5 mg L^{-1}	COF-TpDd	13.88	0.0073	0.9560	18.08	0.0013	0.9981
	COF-TpDb-AO	16.39	0.0101	0.9908	20.16	0.0011	0.9994
	COF-TpDd-AO_2	18.36	0.0089	0.9818	22.98	0.0010	0.9993

Table. S5. The selectivity coefficient of COF-TpDd-AO_2 for uranium; C_0 (uranium) = 5 mg L^{-1} and C_0 (coexisting metals) = 5 and 50 mg L^{-1}.

Element	C_0 (mg L^{-1})	Removal efficiency (%)	Selectivity coefficient $\left(\beta_{UO_2^{2+}/M^{n+}}\right)$
Na^+	5	89.59	53356.10
	50	89.51	69929.39
Mg^{2+}	5	89.61	903.89
	50	89.59	1451.05
Pb^{2+}	5	89.58	4.38
	50	89.60	2037.95
Cd^{2+}	5	89.59	47.86
	50	89.57	234.43
Fe^{3+}	5	89.58	7.32
	50	89.61	0.25☆

☆: The precipitation of Fe^{3+} resulted in an abnormal affinity coefficient.

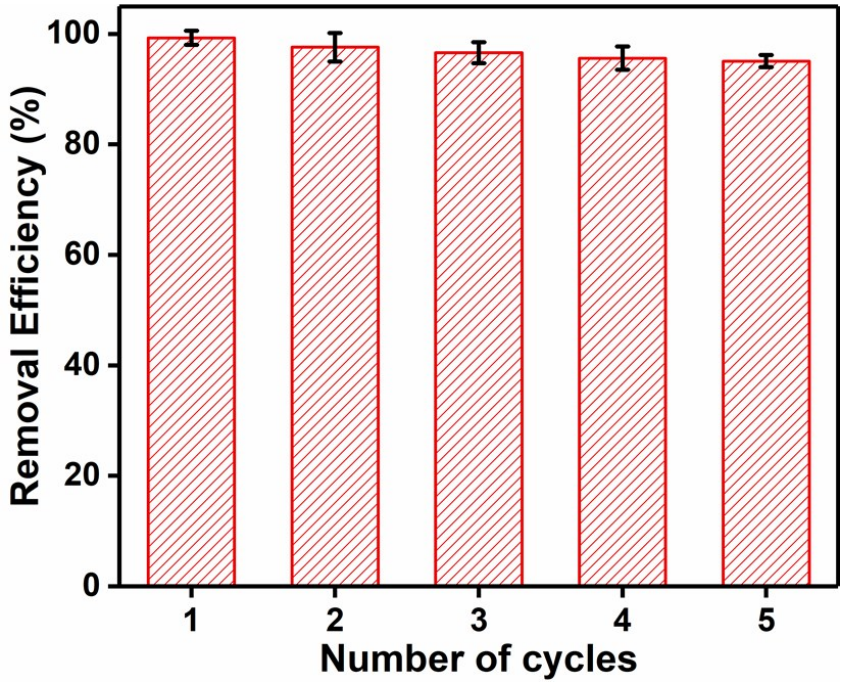

Fig. S5. The adsorption performance of COF-TpDd-AO_2 after five cycles to uranium.

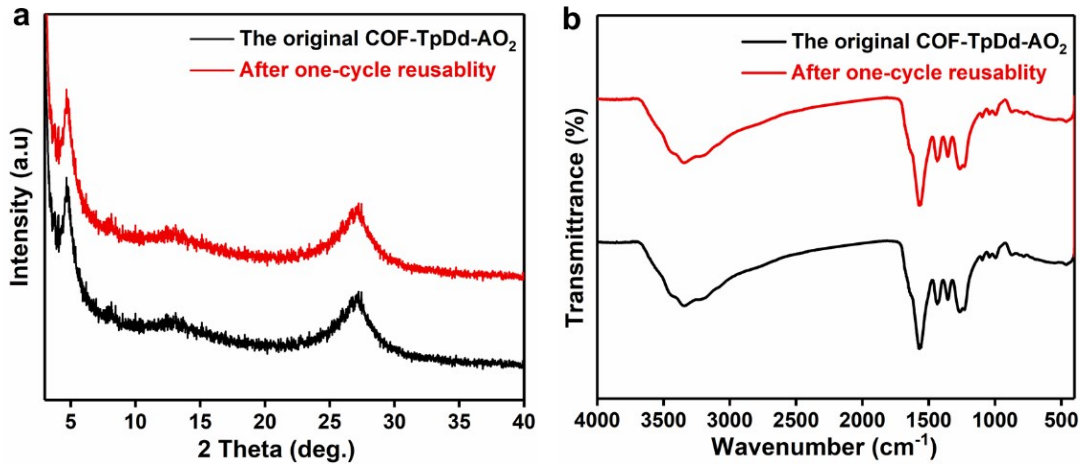

Fig. S6. The XRD (a) and FT-IR spectra (b) of COF-TpDd-AO_2 before and after the first adsorption cycle.

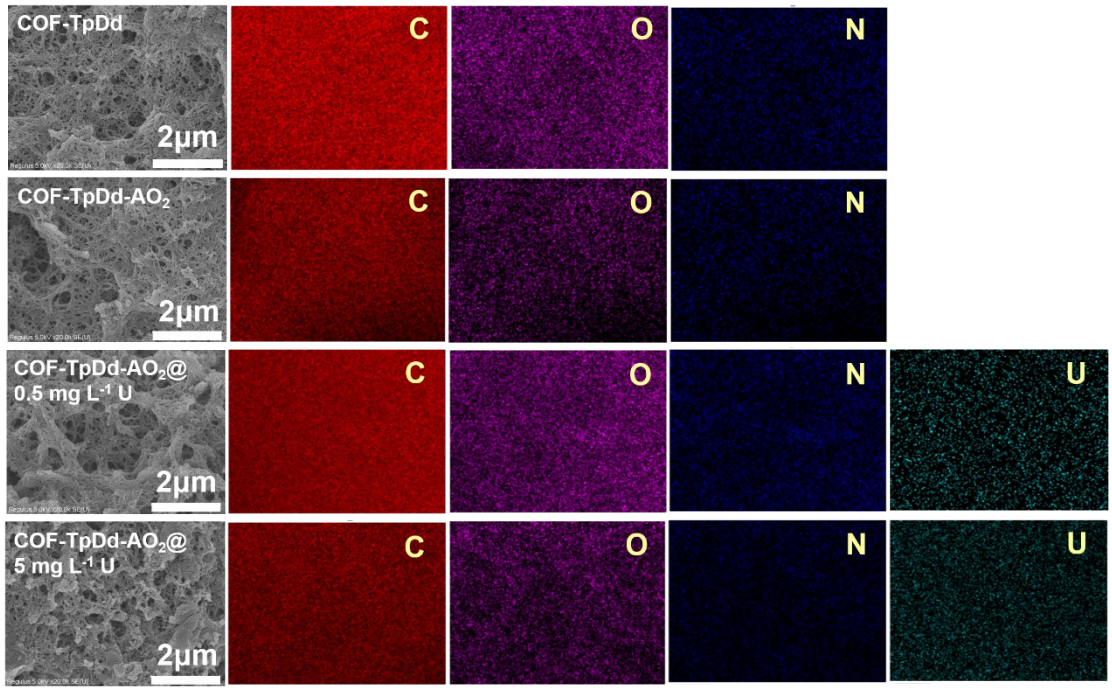

Fig. S7. The SEM image and EDS mapping of COF-TpDd, COF-TpDd-AO_2 and after 0.5 and 5 mg L^{-1} adsorbed by COF-TpDd-AO_2.

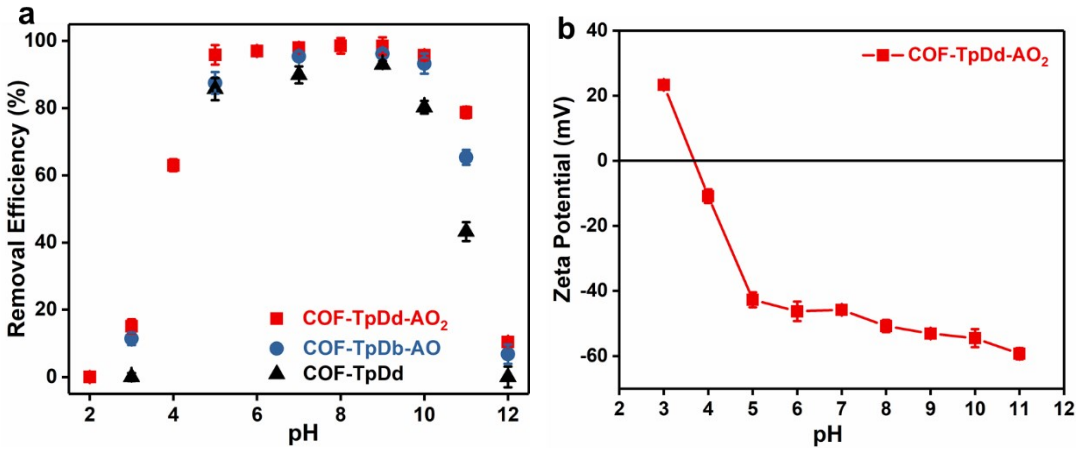

Fig. S8. (a) The effect of pH on adsorption capacity of COFs for uranium; (b) Zeta potentials of COF-TpDd-AO_2 as a function of solution pHs. COFs included COF-TpDd, COF-TpDb-AO, and COF-TpDd-AO_2.

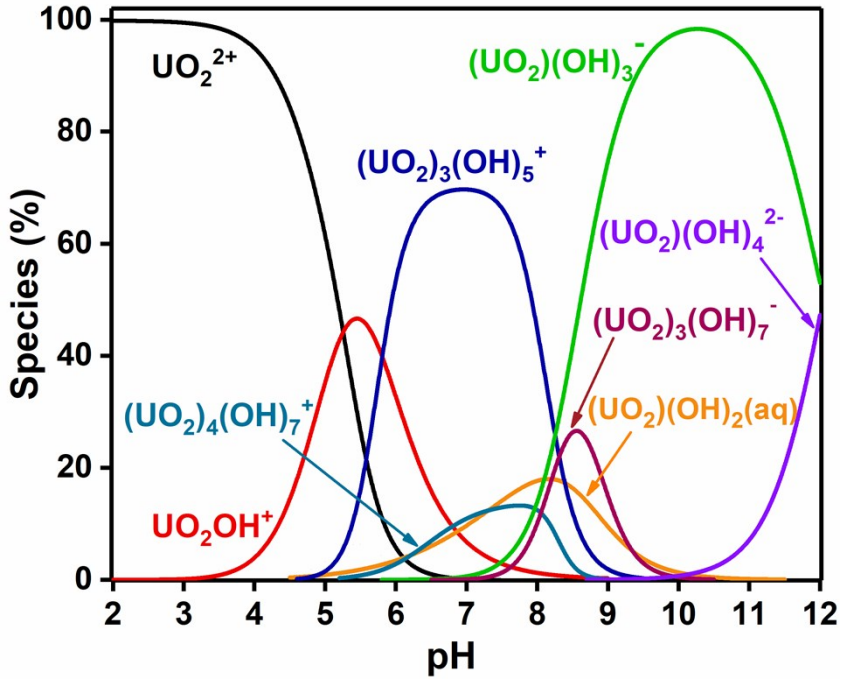

Fig. S9. The species distribution of uranium as a function of pH.

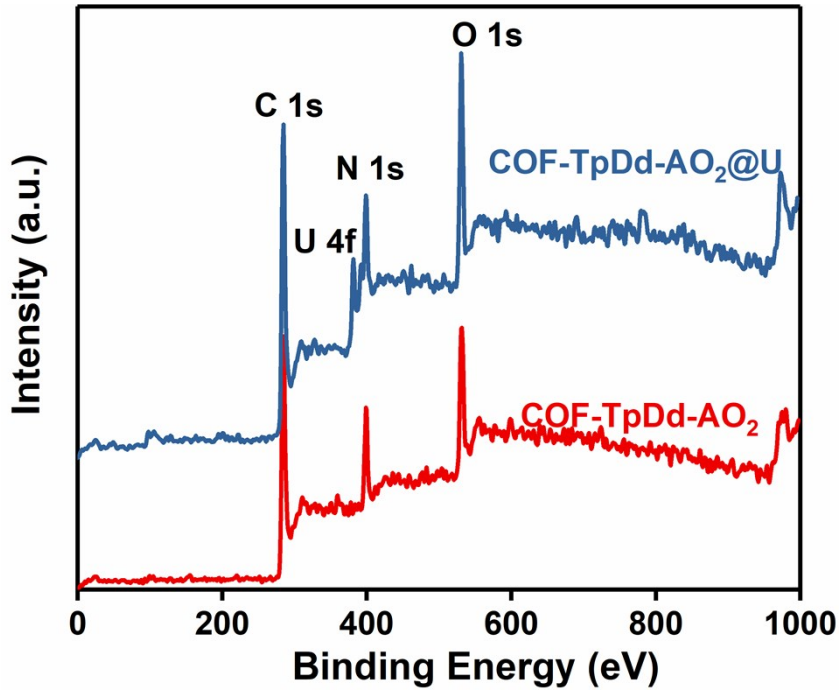

Fig. S10. The XPS spectra of COF-TpDd-AO_2 before and after adsorption.

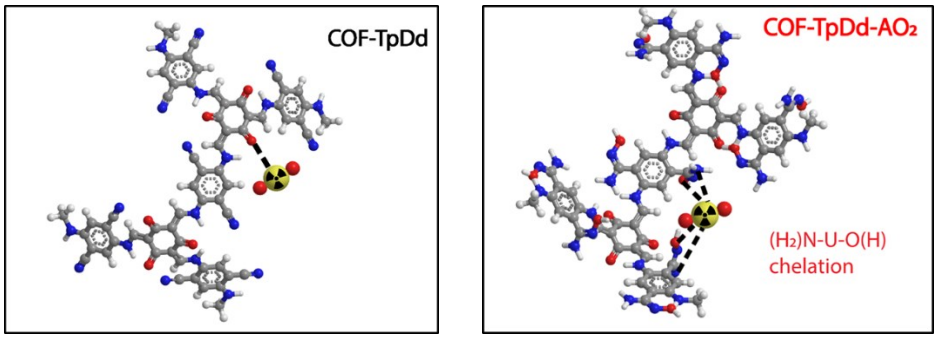

Fig. S11. The comparison of adsorption interaction of COF-TpDd-AO_2 and the pristine COF-TpDd with uranium.

Reference

1. X. Yin, J. Bai, W. Tian, S. Li, J. Wang, X. Wu, Y. Wang, F. Fan, Q. Huang and Z. Qin, Uranium sorption from saline lake brine by amidoximated silica, *J. Radioanal. Nucl. Chem.*, 2017, **313**, 113-121.
2. Q. Sun, B. Aguila, L. D. Earl, C. W. Abney, L. Wojtas, P. K. Thallapally and S. Ma, Covalent organic frameworks as a decorating platform for utilization and affinity enhancement of chelating sites for radionuclide sequestration, *Adv. Mater.*, 2018, **30**, 1705479.
3. X. Li, Y. Qi, G. Yue, Q. Wu, Y. Li, M. Zhang, X. Guo, X. Li, L. Ma and S. Li, Solvent- and catalyst-free synthesis of an azine-linked covalent organic framework and the induced tautomerization in the adsorption of U(VI)) and Hg(II), *Green Chem.*, 2019, **21**, 649-657.
4. F.-F. Li, W.-R. Cui, W. Jiang, C.-R. Zhang, R.-P. Liang and J.-D. Qiu, Stable sp^2 carbon-conjugated covalent organic framework for detection and efficient adsorption of uranium from radioactive wastewater, *J. Hazard. Mater.*, 2020, **392**, 122333.
5. W.-R. Cui, C.-R. Zhang, W. Jiang, F.-F. Li, R.-P. Liang, J. Liu and J.-D. Qiu, Regenerable and stable sp^2 carbon-conjugated covalent organic frameworks for selective detection and extraction of

uranium, *Nat. Commun.*, 2020, **11**, 436.

6. C.-R. Zhang, W.-R. Cui, W. Jiang, F.-F. Li, Y.-D. Wu, R.-P. Liang and J.-D. Qiu, Simultaneous sensitive detection and rapid adsorption of UO_2^{2+} based on a post-modified sp^2 carbon-conjugated covalent organic framework, *Environ. Sci.: Nano.*, 2020, **7**, 842-850.
7. L. He, S. Liu, L. Chen, X. Dai, J. Li, M. Zhang, F. Ma, C. Zhang, Z. Yang, R. Zhou, Z. Chai and S. Wang, Mechanism unravelling for ultrafast and selective $^{99}TcO_4^-$ uptake by a radiation-resistant cationic covalent organic framework: a combined radiological experiment and molecular dynamics simulation study, *Chem. Sci.*, 2019, **10**, 4293-4305.
8. N. Huang, L. Zhai, H. Xu and D. Jiang, Stable covalent organic frameworks for exceptional mercury removal from aqueous solutions, *J. Am. Chem. Soc.*, 2017, **139**, 2428-2434.
9. Q. Sun, B. Aguila, J. Perman, L. D. Earl, C. W. Abney, Y. Cheng, H. Wei, N. Nguyen, L. Wojtas and S. Ma, Postsynthetically modified covalent organic frameworks for efficient and effective mercury removal, *J. Am. Chem. Soc.*, 2017, **139**, 2786-2793.
10. Y. Li, X. Guo, X. Li, M. Zhang, Z. Jia, Y. Deng, Y. Tian, S. Li and L. Ma, Redox-active two-dimensional covalent organic frameworks for selective reductive separation of valence-variable, redox-sensitive and long-lived radionuclides, *Angew. Chem., Int. Ed.*, 2020, **59**, 4168-4175.
11. Y. Li, C. Wang, S. Ma, H. Zhang, J. Ou, Y. Wei and M. Ye, Fabrication of hydrazone-linked covalent organic frameworks using alkyl amine as building block for high adsorption capacity of metal Ions, *ACS Appl. Mater. Interfaces*, 2019, **11**, 11706-11714.